Journal of Materials Science and Chemical Engineering, 2014, 2, 17-32
Published Online August 2014 in SciRes. http://www.scirp.org/journal/msce
http://dx.doi.org/10.4236/msce.2014.28004

P-Doped Titania Xerogels as Efficient UV-Visible Photocatalysts

Céline J. Bodson[1], Sophie L. Pirard[1], René Pirard[1], Ludivine Tasseroul[1], Catherine Bied[2], Michel Wong Chi Man[2], Benoît Heinrichs[1], Stéphanie D. Lambert[1*]

[1]Laboratory of Chemical Engineering—Nanomaterials, Catalysis, Electrochemistry, University of Liege, Liege, Belgium
[2]Charles Gerhardt Montpellier Institute (UMR5253 CNRS-UM2-ENSCM-UM1), Montpellier, France
Email: [*] stephanie.lambert@ulg.ac.be

Received 15 June 2014; revised 27 July 2014; accepted 6 August 2014

Abstract

In the present study, sol-gel process is used to synthesize P-doped TiO_2 xerogels by the cogelation method of a functionalized P alkoxide, $(NH_2\text{-}(CH_2)_2\text{-}NH\text{-}(CH_2)_2\text{-}P(O)\text{-}(OC_2H_5)_2)$ with $Ti(OC_3H_7)_4$ in either 2-methoxyethanol or isopropanol. The phosphorus-doping improved the thermal stability of titania and decreased the phase transformation of anatase into rutile. This modification by phosphorus shifted the absorption edge of titania to the visible region as proved by Diffuse reflectance measurements, and thus offers the possibility to produce visible light effective TiO_2 photocatalyst. The excellent photocatalytic activity of P-doped TiO_2 xerogels compared to pure TiO_2 could be explained by its high surface area and small TiO_2-anatase crystallite size. From these results, it was proved by using three different models that phosphorus intrinsically influences the photocatalytic activity.

Keywords

TiO_2 xerogel, Phosphorus-Doping, Sol-Gel, *p*-Nitrophenol Degradation, Photocatalysis

1. Introduction

TiO_2 heterogeneous photocatalysis is an attractive technique for the complete destruction of undesirable contaminants either in aqueous or gaseous phase by using solar or artificial light illumination [1]-[3]. Upon band gap excitation of TiO_2, the photoinduced electrons and positively charged holes can reduce and oxidize the species adsorbed on the TiO_2 particles. However TiO_2 has several drawbacks among which it can only be activated by

[*]Corresponding author.

How to cite this paper: Bodson, C.J., Pirard, S.L., Pirard, R., Tasseroul, L., Bied, C., Man, M.W.C., Heinrichs, B. and Lambert, S.D. (2014) P-Doped Titania Xerogels as Efficient UV-Visible Photocatalysts. *Journal of Materials Science and Chemical Engineering*, **2**, 17-32. http://dx.doi.org/10.4236/msce.2014.28004

UV light due to its large band gap (E_g = 3.20 eV for anatase) [4] which is energy-consuming and therefore costly. It thus appears interesting to sensitize TiO_2 to the whole visible region which may be achieved by doping with non-metallic atoms such as phosphorus [5]. In this case, a new energy band is created, by the combination between P 3*p* and O 2*p* levels, and is located just below the TiO_2 conduction band [6]. The band gap energy decreases and hence it is easier to create photoinduced electrons and positively charged holes.

In photocatalysis, the cristallinity and the specific surface area of the catalyst are two very important physico-chemical properties. Moreover, there is a close relationship between the adsorption spectrum of the photocatalyst and its efficiency. In the case of TiO_2 xerogels, it is possible to transform an amorphous sample into a crystalline one by calcination under air at an adequate temperature. Indeed, an amorphous TiO_2 sample, synthesized by the sol-gel process and dried at low temperature (≤150˚C), gradually crystallizes into anatase at around 373˚C [7]. Between 550˚C and 750˚C, TiO_2-anatase is irreversibly transformed into the less TiO_2-rutile photoactive phase [8]. Nevertheless, the temperatures of TiO_2 phase transformation (amorphous-anatase and anatase-rutile) are dependent on several parameters: the nature of precursors used for the synthesis [9] [10], the procedure (sol-gel process, hydrothermal synthesis, chemical vapor deposition…) [11] [12] and the insertion of dopants into the TiO_2 matrix [13]-[15].

We recently reported the synthesis of Si-doped and P-doped TiO_2 to produce porous xerogels [16]. The P-doped TiO_2 were synthesized by the cogelation of titanium isopropoxide ($Ti(OC_3H_7)_4$ called TTIP) with a phosphonate compound (diethyl-(2-*N*-(2-aminoethyl)aminoethyl)phosphonate, NH_2-$(CH_2)_2$-NH-$(CH_2)_2$-P(O)-$(OC_2H_5)_2$ called EDAP). In this report, Raman and solid ^{31}P NMR spectroscopies were used to demonstrate the successful formation of Ti-O-P bonds in the dried P-doped titania xerogels. Interestingly it was found that the doping TiO_2 with phosphorus not only evidenced a broadening of the absorption band of titania towards the visible range but it also significantly increases the specific surface area of the materials [16].

In the present work, we synthesized and characterized new P-doped TiO_2 xerogels which were then used as photocatalysts for the degradation of *p*-nitrophenol. The first part is focused on the TG-DSC measurements in order to determine any changes on phase transition due to the phosphorus incorporation into TiO_2 framework. In the second part, the evolution of the physico-chemical properties (specific surface area, cristallinity, absorption properties…) of dried P-doped TiO_2 xerogels with the calcination temperature (350˚C, 450˚C, 550˚C and 650˚C) is presented. To that purpose, the samples have been characterized by ICP-AES, XRD, nitrogen sorption analyses and DR-UV/Vis measurements. The third part of this study is devoted to the study of the photocatalyic activity of all dried and calcined samples particularly for the degradation of *p*-nitrophenol (PN), a model pollutant, under UV-Vis light. It appears that phosphorus has a strong influence on the photocatatytic activity. Such an influence can be due to either to the influence of phosphorus on surface area, crystallite anatase size, and/or intrinsic influence of Ti-O-P bond formation. To distinguish between both effects, three models were developed to find any correlations between activity and physico-chemical properties.

2. Experimental

2.1. Sample Preparation

Four gels were synthesized from TTIP ($Ti(OC_3H_7)_4$), EDAP (NH_2-$(CH_2)_2$-NH-$(CH_2)_2$-P(O)-$(OC_2H_5)_2$) in either 2-methoxyethanol or isopropanol as solvent. The synthesis operating variables are presented in **Table 1**. The molar dilution ratio, D = [solvent]/([TTIP] + [EDAP]), and the molar hydrolysis ratio, H = [H_2O]/([TTIP] + 1/2[EDAP]), were fixed to 20 and 2 respectively for all the samples. For each sample, Met or Iso denotes the solvent used for the synthesis, respectively 2-methoxyethanol and isopropanol; TiP/X denotes TiO_2 xerogels synthesized with EDAP and for which, X is the molar [EDAP]/[TTIP] ratio. Pure TiO_2 xerogel synthesized in 2-methoxyethanol is denoted Met-TiO_2 and was synthesized as blank material for comparison with the P-doped xerogels.

All the syntheses were performed under inert atmosphere (N_2) according to the following steps: 1) after mixing EDAP in half of the total volume of solvent, the slurry was stirred at room temperature for 10 min; 2) then the mixture of TTIP and water in the remaining half of the total ethanol volume was slowly added to the EDAP mixture under vigorous stirring. The volume of the final solutions was 125 mL. The vessel was then tightly closed and heated up to 60˚C for 24 h (gelling and ageing [17]).

Gel time (t_g) is the time elapsed from the introduction of the last reactant in the solution until gelation occured

Table 1. Synthesis operating variables of P-doped TiO_2 xerogels.

Sample	n_{EDAP} (mmol)	n_{TTIP} (mmol)	n_{H_2O} (mmol)	$n_{solvent}$ [a] (mmol)	Theoretical [EDAP]/[TTIP] (mol/mol)	Actual [EDAP]/[TTIP] [b] (mol/mol)	t_g [c] (min)
Met-TiO_2	-	65.0	130	1330	-	-	8
Met-TiP/0.01	0.61	67.2	130	1330	0.01	0.009	18
Met-TiP/0.1	6.09	62.2	130	1330	0.10	0.114	28
Iso-TiP/0.1	6.09	62.2	130	1331	0.10	0.097	12

[a] $n_{solvent}$ is 2-methoxyethanol or isopropanol. [b] measured by ICP-AES. [c] t_g is the gel time.

and was performed in an oven at 60˚C. Gelation is defined as the point when the liquid does not flow anymore when the flask is tipped at an angle of 45˚.

The wet gels were dried under vacuum according to the following procedure: the flasks were opened and placed into a drying oven at 60˚C, and the pressure was slowly decreased (to prevent gel bursting) to the minimum value of 1200 Pa after 48 h. The drying oven was then heated at 150˚C for 24 h leading to xerogels [17].

Each sample is divided in four parts with the same mass. Each part is calcined at a different temperature, *i.e.* 350˚C, 450˚C, 550˚C and 650˚C, as follows: the sample was heated up to the desired temperature at a rate of 150˚C/h under flowing air (0.0074 mol·s^{-1}); this temperature was maintained for 5 h in air (flow rate: 0.02 mol·s^{-1}). Calcined samples are denoted Met-TiP/X-T or Iso-TiP/X-T, where T is the calcination temperature of the sample. For example, Met TiP/0.1-550 is a P-doped TiO_2 xerogel synthesized in 2-methoxyethanol, with a molar [EDAP]/[TTIP] ratio = 0.1, and calcined at 550˚C under air for 5 h.

2.2. Sample Characterization

Inductively coupled plasma-atomic emission spectroscopy (ICP-AES), equipped with an ICAP 6500 THERMO Scientific device was used to determine the molar [EDAP]/[TTIP] ratio of the dried and calcined samples of P-doped TiO_2 xerogels. Solutions for analysis were prepared as follows: 1) 2 g of Na_2O_2, 1 g of NaOH and 0.1 g of sample were mixed in a vitreous carbon crucible; 2) the mixture was heated beyond the melting point (up to 950˚C); 3) after cooling and solidification, the mixture was digested in 30 mL of HNO_3 (65%); 4) the solution was then transferred into a 500 mL calibrated flask that was finally filled with deionized water. The measured molar [EDAP]/[TTIP] ratio for dried P-doped TiO_2 xerogels are given in **Table 1** and the measured molar [EDAP]/[TTIP] ratio for calcined P-doped TiO_2 xerogels are given in **Table 2**.

TG-DSC measurements were realized under helium between 40˚C and 700˚C, with a heating rate of 0.16˚C·s^{-1}, using a Setaram TG-DSC 111 device, according to the following procedure: 1) a precise amount of sample was placed into a platinum crucible; 2) the sample was heated under helium from 40˚C to 700˚C; 3) the sample was cooled and was weighed again.

X-ray diffraction (XRD) patterns were recorded with a Siemens D5000 powder diffractometer (Cu-K_α radiation) between 20˚ and 65˚ (2θ). The size of TiO_2-anatase particles, d_a, was estimated from X-ray peak broadening by the Scherrer method [18].

Nitrogen adsorption-desorption isotherms were measured at −196˚C on a Fisons Sorptomatic 1990 after outgassing (10^{-5} Pa) for 24 h at room temperature.

Diffuse reflectance measurements in the UV/Vis region (250 - 800 nm) (DR-UV/Vis) were performed on a Varian Cary 5000 UV/Vis/NIR spectrophotometer, equipped with a Varian External DRA-2500 integrating sphere, using $BaSO_4$ as reference. Samples have been prepared by immobilizing the powder between a PVC support and a quartz glass. UV/Vis spectra were recorded in diffuse reflectance mode (R = reflection intensity) and transformed to the absorbance coefficient (F(R)) by the Kubelka-Munk function [19], $F(R) = (1-R)^2 / 2R$. The illuminated surface is the same for all samples. For the sake of comparison, all spectra were arbitrary normalized in intensity to 1.0 by dividing each spectrum by their maximum. The band gap has been determined from the Tauc plot [20] $(F(R)h\nu)^{1/2}$ versus hν.

2.3. Photocatalytic Tests

The photoactivity of the xerogels was compared by evaluating the relative residual concentration of *p*-nitro-

Table 2. Actual molar [EDAP]/[TTIP] ratio measured by ICP-AES for P-doped TiO_2 xerogels.

Sample	[EDAP]/[TTIP] (mol/mol)
Met-TiP/0.01	0.0089
Met-TiP/0.01-350	0.0088
Met-TiP/0.01-450	0.0087
Met-TiP/0.01-550	0.0028
Met-TiP/0.01-650	0.0056
Met-TiP/0.1	0.1145
Met-TiP/0.1-350	0.1098
Met-TiP/0.1-450	0.1123
Met-TiP/0.1-550	0.0710
Met-TiP/0.1-650	0.0724
Iso-TiP/0.1	0.0971
Iso-TiP/0.1-350	0.0982
Iso-TiP/0.1-450	0.0964
Iso-TiP/0.1-550	0.0932
Iso-TiP/0.1-650	0.0246

phenol (PN) after 6 h under the halogen lamp. The photocatalytic degradation of PN was carried out using a batch reactor with an external halogen lamp (Philips 300 W, 240 V). A circulating water jacket was used to cool the batch reactor and the temperature was kept at 23˚C. The photocatalytic degradation of PN was realized in 8 closed tubes disposed in water around the lamp. Each suspension (volume = 15 mL) in each tube was mixed under vigorous stirring.

In a typical experiment, the catalyst was added to 15 mL aqueous solution of PN (Initial concentration, C_i, is equal to 10^{-4} mol·L^{-1}) to reach a concentration of 1 g·L^{-1}. To degrade only the protonated form of PN (pK_a = 7.2), the solution pH was fixed at 3.5 by adding a few µL of 1 N HCl aqueous solution. The shaking of the suspension was controlled during the photocatalytic test to ensure that the suspension was homogeneous. Time 0 corresponds to the switching on of the lamp. After 6 h, 2 mL of each suspension were sampled with a syringe and filtered in order to separate the xerogel powder from the *p*-nitrophenol solution. In those experimental conditions, the pH of the filtered *p*-nitrophenol solution was equal to 4. Therefore, only the protonated form of *p*-nitrophenol was present in the solution. The final concentration of that protonated form of *p*-nitrophenol, C_f, was measured by UV/Vis spectroscopy (Genesys 10S UV-Vis, Thermo Scientific) at 318 nm. The photocatalytic activity of samples was calculated from the percentage of PN degraded after 6 h, *A*, and given by Equation (1):

$$A = \left(C_i - C_f\right)/C_i \times 100 \quad (1)$$

where C_i is the initial PN concentration and C_f is the final PN concentration after 6 h. The same experimental protocol was applied to a solution containing PN only, that is without xerogel under light and to PN solution containing each xerogel successively but without light to ensure that the relative residual concentration obtained corresponds really only to the photodegradation of PN by pure TiO_2 and P-doped TiO_2 xerogels under halogen lamp. Each measurement was repeated three times.

2.4. Parameters Estimation and Statistical Testing of Models

The fitting of kinetic models was performed by applying the Gauss-Newton optimization method by using a statistical Fisher *F*-test [21] [22]. NLPE software, Non Linear Parameter Estimation, from IBM was used [23].

3. Results

3.1. Thermogravimetric Behaviour of Pure TiO_2 and P-Doped TiO_2 Xerogels

In **Figure 1(a)**, TG-DSC curves are presented for the sample Met-TiO_2. A weight loss of about 20% associated

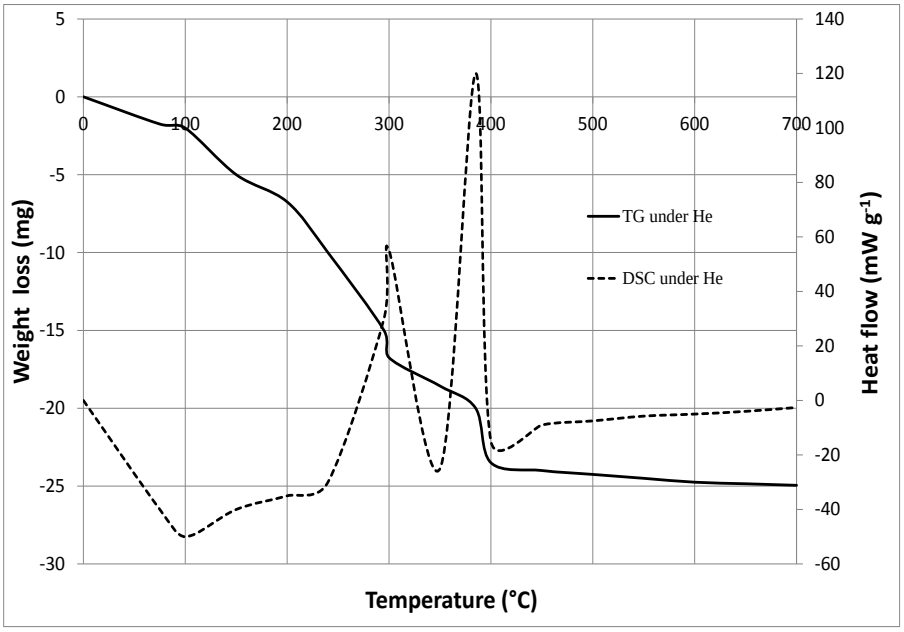

(a)

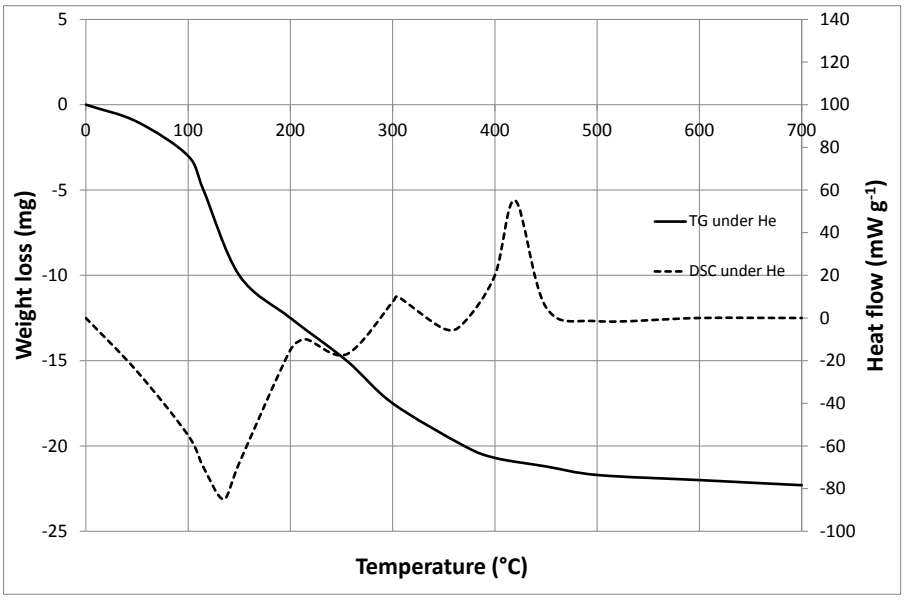

(b)

Figure 1. TG-DSC curves of (a) sample Met-TiO_2 (initial weight = 73.2 mg) and (b) sample Met-TiP/0.01 (initial weight = 70 mg).

to a large endothermic peak is observed between 50˚C and 250˚C, corresponding to the evaporation of 2-methoxyethanol and water. The weight loss (for a total of about 28%) extends to 450˚C with two exothermic phenomena at 300˚C and 385˚C. In that temperature range it is known that the condensation reactions occur in the solid and thus these exothermic phenomena can be attributed to the condensation between hydroxyl groups or between hydroxyl groups and remaining alkoxy groups associated to the formation of water or alcohol and to the weight losses [24].

Moreover, the cristallization of amorphous TiO_2 into anatase is also an exothermic phenomenon which occurs at around 373˚C [7]. The peak corresponding to this transformation probably overlaps with the second peak at 385˚C and associated to one of the condensation reactions.

Figure 1(b) represents the TG-DSC curves of the sample Met-TiP/0.01. A weight loss of about 20% associated to a large endothermic peak is observed between 30˚C and 210˚C, corresponding to the evaporation of 2-methoxyethanol and water. The weight loss (for a total of about 32%) extends to 500˚C with one endothermic peak at 250˚C following by two exothermic phenomena at 300˚C and 410˚C. The endothermic peak at 250˚C could correspond to residual 2-methoxyethanol pyrolysis. As in the former case, both exothermic peaks are attributed to the condensation reactions [25]. Nevertheless, the first exothermic peak at 300˚C is smaller in **Figure 1(b)** than in **Figure 1(a)**. This peak mitigation could correspond to the formation of P_2O_5 species from EDAP, which sublimes at around 300˚C and which is an endothermic phenomenon [24]. Moreover, the second exothermic peak at 420˚C could correspond to the cristallization of amorphous TiO_2 into anatase, but with a delay of about 40˚C.

Both samples Met-TiP/0.1 and Iso-TiP/0.1 (curves not shown) exhibit similar TG-DSC curves under He as sample Met-TiP/0.01. Nevertheless, the second exothermic peak appears at markedly higher temperature (550˚C) instead of 420˚C for sample Met-TiP/0.01 and instead of 385˚C for sample Met-TiO_2. We may thus conclude that the presence of phosphorus into TiO_2 matrix delays the crystallization of amorphous TiO_2 into anatase, an incremental crystallization delay being observed with increasing phosphorus loading.

3.2. X-Ray Diffraction of Pure TiO_2 and P-Doped TiO_2 Xerogels

The effect of calcination temperature on sample crystallinity was investigated by X-ray diffraction. The XRD patterns of the sample Met-TiO_2 (curves not shown) display only anatase reflections (JCPDS 21-1272: 2θ = 25.3˚, 37.9˚, 48.0˚, 54.6˚ et 62.8˚) after calcination at 350˚C, 450˚C and 550˚C. When the sample Met-TiO_2 is heated up to 650˚C, it undergoes a phase transition from anatase structure to rutile structure (JCPDS 21-1276: 2θ = 27.3˚, 35.9˚, 41.1˚ et 54.1˚) as already reported in literature [15].

The XRD patterns of sample Met-TiP/0.01 calcined at 350˚C, 450˚C, 550˚C and 650˚C are presented in **Figure 2** and exemplifies those of samples Met-TiP/0.01, Met-TiP/0.1 and Iso-TiP/0.1 which follow the same trend. After calcination at 350˚C and 450˚C, the sample Met-TiP/0.01 is always amorphous. When the calcination temperature is ≥550˚C, the characteristic peaks of anatase structure appear on the patterns. Nevertheless, even after a calcination at 650˚C for 5 h, no rutile structure appears on the patterns of samples Met-TiP/0.01, Met-TiP/0.1 and Iso-TiP/0.1.

The TiO_2 anatase crystallite sizes, d_a, calculated by the Scherrer equation from peak broadening [18] are presented in **Table 3** for all the samples. It is observed that d_a increases with the calcination temperature. Interestingly, by comparing samples Met-TiP/0.01 with Met-TiP/0.1, it is obvious that the nanoparticle size, d_a, increases more slowly, and thus the cristallization of amorphous TiO_2 into anatase structure is more delayed in the latter case with a higher phosphorus loading increases. This is confirmed with sample Iso-TiP/0.1 which exhibits similar sizes as Met-TiP/0.1.

3.3. Nitrogen Adsorption-Desorption Isotherms of P-Doped TiO_2 Xerogels

The textural properties of P-doped TiO_2 xerogels are reported in **Table 4**. Those of sample Met-TiO_2 are not given in this table because it is not porous (S_{BET} < 5 $m^2 \cdot g^{-1}$) whichever the calcination temperature (350˚C, 450˚C, 550˚C and 650˚C).

In **Figure 3(a)**, nitrogen adsorption-desorption isotherms of sample Met-TiP/0.01 dried and calcined at 350˚C, 450˚C, 550˚C and 650˚C are presented. Like sample Met-TiO_2, the dried sample Met-TiP/0.01 is not porous. One reason could be the presence of the organic aminoethylaminopropyl chain of EDAP in the pores thus reducing accessibility to the latter ones and this is also shown in **Table 4** with a specific surface area, S_{BET}, of <5 $m^2 \cdot g^{-1}$. After calcination under air at 350˚C, the isotherm of the resulting sample Met-TiP/0.01-350 exhibits a narrow adsorption-desorption hysteresis loop for p/p_0 values between 0.4 and 0.6 characteristic of capillary condensation in small mesopores (2 - 10 nm) [26]. Indeed, in **Table 4**, the specific surface area obtained from the Broekhoff-de-Boer theory and characteristic of the presence of mesopores, S_{BdB}, is equal to 90 $m^2 \cdot g^{-1}$, while S_{BET} of this sample is equal to 115 $m^2 \cdot g^{-1}$ showing that sample Met-TiP/0.01-350 is essentially mesoporous. Nevertheless, this sample is also slightly microporous because the microporous volume calculated from the Dubinin-Raduskevitch theory, V_{DR}, is equal to 0.04 $cm^3 \cdot g^{-1}$. Upon calcination under air at 450˚C (**Figure 3(a)**), the adsorption-desorption hysteresis loop is shifted towards higher p/p_0 values, resulting from an increase of the size of the mesopores [26]. In **Table 4**, S_{BET} and S_{BdB} for the sample Met-TiP/0.01-450 decrease down to 65 $m^2 \cdot g^{-1}$

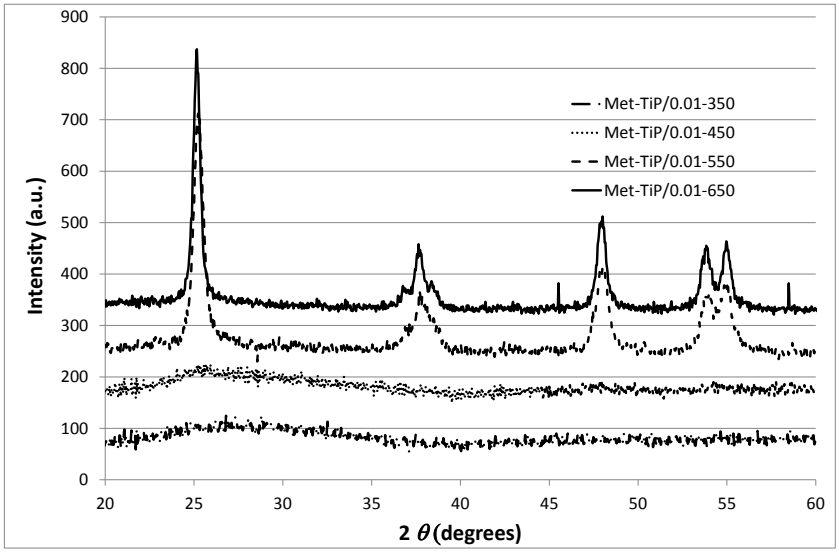

Figure 2. X-ray diffraction patterns of sample Met-TiP/0.01-T calcined at 350˚C, 450˚C, 550˚C and 650˚C.

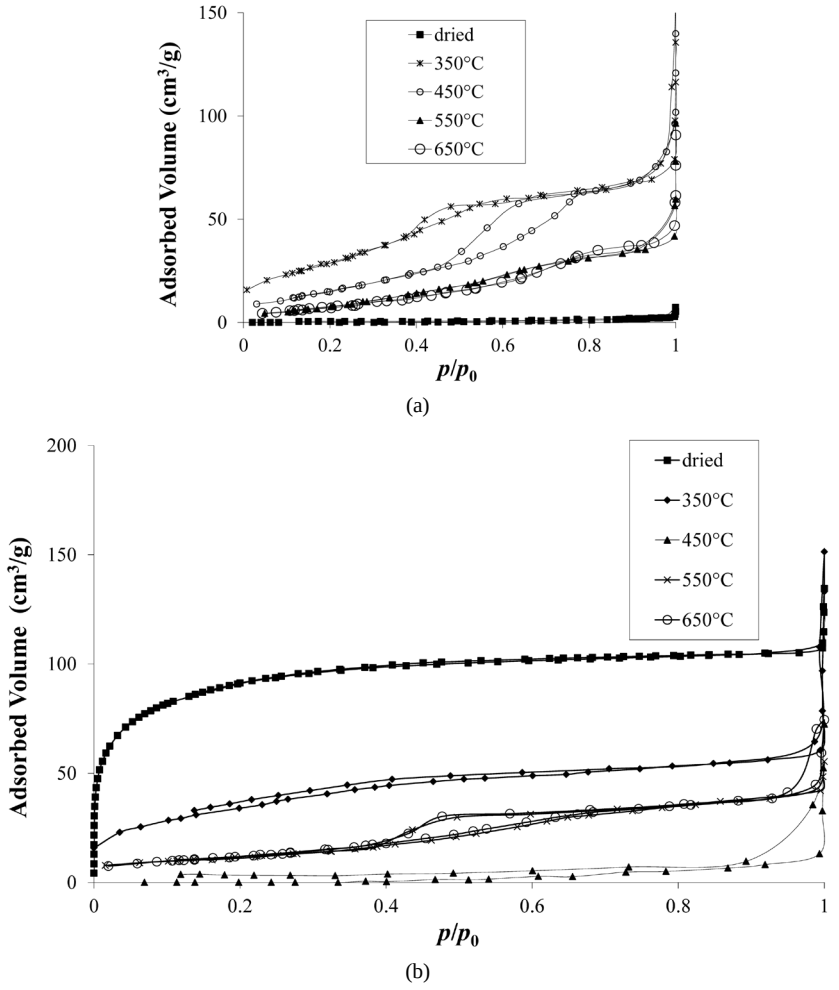

Figure 3. Nitrogen adsorption-desorption isotherms of (a) sample Met-TiP/0.01-T and (b) sample Iso-TiP/0.1-T.

Table 3. TiO_2 anatase crystallite sizes as a function of calcination temperature.

Calcination temperature (˚C)	d_a (nm)			
	Met-TiO_2	Met-TiP/0.01	Met-TiP/0.1	Iso-TiP/0.1
350	8	-[a]	-[a]	-[a]
450	11	6	6	-[a]
550	24	15	8	9
650	R	19	8	11

[a]not measurable; R = rutile.

Table 4. Textural properties of P-doped TiO_2 xerogels.

Sample	S_{BET} ±5 ($m^2 \cdot g^{-1}$)	S_t ±5 ($m^2 \cdot g^{-1}$)	S_{BdB} ±5 ($m^2 \cdot g^{-1}$)	V_p ±0.1 ($cm^3 \cdot g^{-1}$)	V_{DR} ±0.01 ($cm^3 \cdot g^{-1}$)
Met-TiP/0.01	<5	<5	-[a]	<0.1	-[a]
Met-TiP/0.01-350	115	115	90	0.2	0.04
Met-TiP/0.01-450	65	70	55	0.2	0.03
Met-TiP/0.01-550	40	40	35	0.1	0.02
Met-TiP/0.01-650	35	35	35	0.1	0.01
Met-TiP/0.1	<5	<5	<5	<0.1	-[a]
Met-TiP/0.1-350	<5	<5	<5	<0.1	-[a]
Met-TiP/0.1-450	70	70	55	0.1	0.03
Met-TiP/0.1-550	105	105	85	0.1	0.04
Met-TiP/0.1-650	90	95	75	0.2	0.04
Iso-TiP/0.1	340	355	100	0.2	0.13
Iso-TiP/0.1-350	125	125	45	0.2	0.06
Iso-TiP/0.1-450	<5	<5	<5	0.2	-[a]
Iso-TiP/0.1-550	40	45	30	0.1	0.02
Iso-TiP/0.1-650	45	45	30	0.1	0.02

[a]not measurable. S_{BET}: specific surface area obtained by BET method; S_t: specific surface area obtained from the slope before the downward deviation in the *t*-plot; S_{BdB}: specific surface area obtained from the Broekhoff-de-Boer theory; V_p: specific liquid volume adsorbed at saturation pressure of nitrogen; V_{DR}: microporous volume calculated from the Dubinin-Raduskevitch theory.

and 55 $m^2 \cdot g^{-1}$ respectively. Their decrease could be due to the beginning of the crystallization of amorphous TiO_2 into anatase (**Figure 2**) [15]. After calcination at 550˚C and 650˚C, mesoporosity is partly maintained but microporosity disappears with similar values of S_{BET} and S_{BdB} (**Table 4**). These samples still present S_{BET} values around 35 - 40 $m^2 \cdot g^{-1}$.

The data from **Table 4**, show that samples of dried Met-TiP/0.1 and Met-TiP/0.1-350 are not porous (S_{BET} < 5 $m^2 \cdot g^{-1}$). After calcination at 450˚C, porosity appears within the sample with S_{BET} and S_{BdB} reaching 70 $m^2 \cdot g^{-1}$ and 55 $m^2 \cdot g^{-1}$ respectively. Further calcination to 550˚C, results in an increase of S_{BET} and S_{BdB} to 105 $m^2 \cdot g^{-1}$ and 85 $m^2 \cdot g^{-1}$ respectively. At this temperature, the anatase structure is not yet well developed (**Table 3**, in which d_a is equal to 8 nm). Upon calcination at 650˚C, S_{BET} and S_{BdB} slightly decrease to 90 - 95 $m^2 \cdot g^{-1}$. Indeed, in **Table 3**, d_a gradually increases because the crystallization of amorphous TiO_2 into anatase structure starts at this stage. The comparison between samples Met-TiP/0.01 and Met-TiP/0.1 shows that the crystallization of amorphous TiO_2 into anatase structure is shifted towards higher temperatures when the phosphorus loading increases, and correlate with the TG-DSC measurements (see 3.1).

In **Figure 3(b)**, nitrogen adsorption-desorption isotherms of samples Iso-TiP/0.1 dried and calcined at 350˚C, 450˚C, 550˚C and 650˚C are presented. The dried sample Iso-TiP/0.1 presents at low relative pressure, a sharp increase of the adsorbed volume, followed by a plateau which corresponds to type I isotherm according to BDDT

classification [26], which is characteristic of microporous adsorbents. Compared with samples Met-TiP/0.01 and Met-TiP/0.1, the specific surface area, S_{BET}, of the dried sample Iso-TiP/0.1 (**Table 4**) is significantly high (340 $m^2 \cdot g^{-1}$). Nevertheless, after calcination at 350˚C, S_{BET}, S_{BdB}, and V_{DR} strongly decrease and the calcination at 450˚C induces the collapse of the texture of the sample with very low surface area (S_{BET} < 5 $m^2 \cdot g^{-1}$). After calcination at 550˚C and 650˚C, amorphous TiO_2 crystallizes into anatase structure with d_a equal to 9 and 11 nm respectively (**Table 3**). In this case, S_{BET} of samples Iso-TiP/0.1-550 and Iso-TiP/0.1-650 is equal to around 40 - 45 $m^2 \cdot g^{-1}$, and the isotherms exhibit similar narrow adsorption-desorption hysteresis loop for p/p_0 values between 0.4 and 0.6. This hysteresis is characteristic of capillary condensation in small mesopores (2 - 10 nm) [26], located between TiO_2 crystallites [15].

3.4. UV/Vis Diffuse Reflectance (DR-UV/Vis) of Pure TiO_2 and P-Doped TiO_2 Xerogels

The DR-UV/Vis spectra of some calcined samples (Met-TiO_2-650, Met-TiP/0.01-550, Met-TiP/0.1-550 and Met-TiP/0.1-650) are given in **Figure 4**: the other samples calcined at 550˚C and 650˚C are not shown as they are very similar. The DR-UV/Vis spectra of those samples of Met-TiO_2, Met-TiP/0.01, Met-TiP/0.1 and Iso-TiP/0.1 calcined at 350˚C and 450˚C are not considered since they still contain a lot of organic moieties as illustrated by their coloured feature. Thus, it is difficult to analyze the DR-UV/Vis spectra of these samples because their absorption in the visible range is higher than the samples calcined at 550˚C and 650˚C [27].

Figure 4 clearly demonstrates that the introduction of phosphorus into TiO_2 matrix induces a shift of the TiO_2 maximal absorption band from 335 nm (Met-TiO2-650) to 370 nm for all the EDAP-containing samples calcined at 550˚C and 650˚C. The molar [EDAP]/[TTIP] ratio (0.01 or 0.1) and the solvent (2-methoxyethanol or isopropanol) have no significant influence on the DR-UV/Vis spectra of the P-doped TiO_2 xerogels.

The calculated band gap energy values are reported in **Table 5**. All P-doped TiO_2 xerogels have a smaller band gap energy values (3.03 - 3.10 eV) than those of samples Met-TiO2-550 and Met-TiO2-650 (respectively 3.55 and 3.42 eV). Here also, the synthesis operating variables (molar [EDAP]/[TTIP] ratio, solvent nature and calcination temperature) have no influence on the band gap energy values.

3.5. Photocatalytic Tests with Pure TiO_2 and P-Doped TiO_2 Xerogels

The photocatalytic activity of the TiO_2 xerogels (pure and P-doped) examined for the PN degradation is presented in **Figure 5** which firstly shows that all dried samples are inactive. With calcination the efficiency of the resulting materials highly increases reaching a maximum of 57% in the case of sample Met-TiP/0.1-650. It also appears that phosphorus has a strong influence on the photocatatytic activity.

4. Discussion

4.1. Thermal Evolution of Pure TiO_2 and P-Doped TiO_2 Xerogels

From TG-DSC measurements, the thermogravimetric behaviour of pure TiO_2 and P-doped TiO_2 xerogels was studied and allowed to define the different temperatures of calcination for samples. Nevertheless, since the operating variables between TG-DSC measurements and calcination are not strictly the same (heating rate, length of the temperature bearing, He for TG-DSC and air for calcination), the temperatures, for which thermal behaviours are examined, can be different for both cases [28].

For the blank Phophorus-free sample Met-TiO_2, the TG-DSC and XRD measurements show three successive thermal behaviours: 1) the solvent and water, which are always present inside the pores of this sample even after drying under vacuum at 150˚C for 24 h, are evaporated below 250˚C, which corresponds to an important weight loss of sample (about 20%); 2) the crystallization of amorphous TiO_2 into anatase occurs at around 380˚C [7] [15]; 3) the crystallization of anatase into rutile seems likely to occur between 550˚C and 650˚C [15]. Furthermore, two exothermic peaks at 300˚C and 385˚C (overlapping with the peak of crystallization of amorphous TiO_2 into anatase) are present in **Figure 1(a)**. These peaks are assigned to condensation reactions between hydroxyl groups or between hydroxyl groups and alkoxy groups [24]. The condensation in the gel is therefore not complete after 24 h at 60˚C (gelling and aging [17]). Indeed, Bodson *et al.* [16], showed that 2-methoxyethanol used as solvent, can also act as a chelating ligand and hence the formation of chelated Ti-species by ligand exchange (Equation (2)) is expected. These are less reactive towards hydrolysis and condensation reactions.

$$\mathrm{Ti}\left(\mathrm{O}-{}^{\mathrm{i}}\mathrm{Pr}\right)_{\mathrm{n}}\left(\mathrm{OEtOMe}\right)_{4-\mathrm{n}}+\mathrm{MeOEtOH}\leftrightarrow\mathrm{Ti}\left(\mathrm{O}-{}^{\mathrm{i}}\mathrm{Pr}\right)_{\mathrm{n}-1}\left(\mathrm{OEtOMe}\right)_{5-\mathrm{n}}+{}^{\mathrm{i}}\mathrm{PrOH}\quad \mathrm{n}=1\text{ to }4 \tag{2}$$

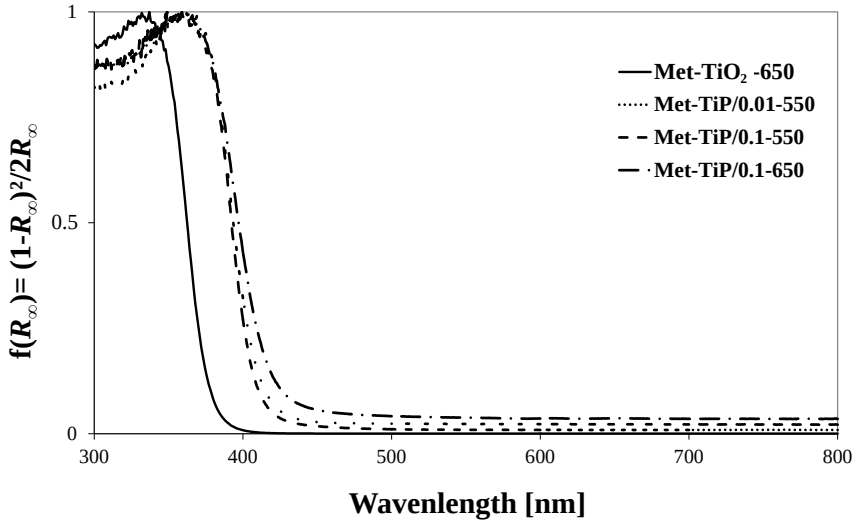

Figure 4. DR-UV/Vis spectra of pure TiO_2 and P-doped TiO_2 xerogels.

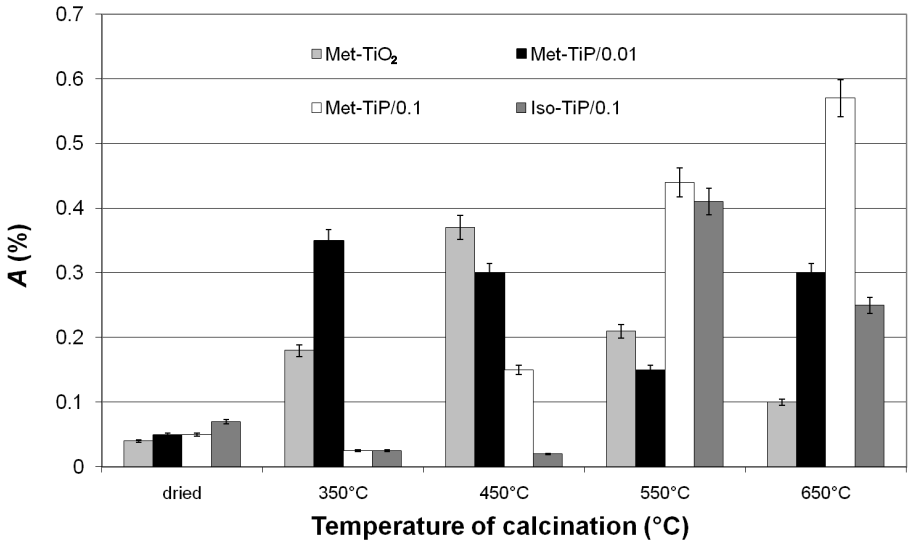

Figure 5. Percentage of PN degradation. pH = 3.5; 6 h of illumination.

Table 5. Band-gap energy (eV) calculated for all samples calcined at 550˚C and 650˚C.

Sample	Met-TiO_2	Met-TiP/0.01	Met-TiP/0.1	Iso-TiP/0.1
Temperature (˚C)				
550	3.55	3.10	3.05	3.10
650	3.40	3.05	3.00	3.10

Considering the P-doped samples (Met-TiP/0.01, Met-TiP/0.1 and Iso-TiP/0.1), the introduction of phosphorus modifies the crystallization temperatures of TiO_2 (**Figure 1(b)** and **Figure 2**): 1) the exothermic peak corresponding to the crystallization of amorphous TiO_2 into anatase, appears at significantly high temperature (550˚C) for the samples with higher phosphorus content (Met-TiP/0.1 and Iso-TiP/0.1); this crystallization temperature decreases to 420˚C for sample Met-TiP/0.01 and is even lower (385˚C) for the P-free sample Met-TiO_2. It is clear that the presence of phosphorus in the TiO_2 matrix delays the transformation of amorphous TiO_2 into crystalline anatase. A longer crystallization delay is observed on increasing the phosphorus loading [5] [27]. Nevertheless, the nature of solvent (2-methoxyethanol or isopropanol) has no influence on the TiO_2 crystalliza-

tion temperature; 2) even after calcination at 650˚C, no rutile phase is detected in P-doped TiO_2 xerogels, contrarily to the sample Met-TiO_2, for which the rutile phase is detected when calcined at 650˚C [15]. These results were also observed by Körösi *et al.* [28] for P-doped TiO_2 materials with molar P/Ti ratios = 0.01 and 0.1. The presence of phosphorus stabilizes the anatase structure, which is very interesting since anatase is the most effective structure of TiO_2 in photocatalysis. Previously, H_3PO_4-doped TiO_2 xerogels were reported and in this case, the rutile structure is obtained for temperatures > 900˚C with a molar P/Ti ratio of 0.05, and >1000˚C with a molar P/Ti ratio of 0.1 to 0.5 [29].

Myller *et al.* [30] showed that [2-(aminoethyl)dihydrogeno]phosphate and [2-(aminoethyl)hydrogenoammonium]phosphate, two similar molecules to EDAP, are decomposed around 300˚C - 350˚C in P-doped TiO_2 materials when these molecules are free and not bonded to TiO_2. In Bodson *et al.* [16], it was shown by Raman and Solid ^{31}P NMR spectroscopies, that the EDAP fragment is maintained within the TiO_2 structure, either by complexation of titanium atoms with the ethylenediamine fragment of EDAP, or by covalent linkage through P-O-Ti bonds. So EDAP molecules only complexed to titanium atoms can sublimate when temperature increases. These results are confirmed by ICP-AES measurements (**Table 2**), for which a loss of phosphorus is observed for all P-doped TiO_2 xerogels when the calcination temperature increases.

It is observed that the size of TiO_2-anatase crystallites, d_a, increases with the calcination temperature for all the samples (**Table 3**). But the growth of TiO_2-anatase crystallites slows down when the molar P/Ti ratio increases [31]. Indeed, after calcination at 650˚C, d_a is equal to 19 nm for the sample Met-TiP/0.01-650, while d_a is around 10 nm for the samples Met-TiP/0.1-650 and Iso-TiP/0.1-650.

In opposite to the nitrogen adsorption-desorption measurements for dried P-doped TiO_2 xerogels [15], the nature of solvent (2-methoxyethanol or isopropanol) is not the key factor, which influences the porous texture of xerogels (**Table 4**). In this work, it seems that the molar P/Ti ratio is the more important factor. Such an influence can be due to either to the influence of phosphorus on surface area, crystallite anatase size, and/or intrinsic influence of Ti-O-P bond formation. To distinguish between both effects, three models are developed below to find any correlations between activity and physico-chemical properties.

4.2. Parameter Adjustment

After examination of **Figure 5** representing the activity of pure TiO_2 and P-doped TiO_2 xerogels for the PN degradation, it is not possible to determine what are the physico-chemical properties—the phosphor rate, the anatase crystallite size and the specific area—that intrinsically influence the phosphor doped TiO_2 xerogel activity. In order to establish correlations between the phosphor rate, the anatase crystallite size, the specific area and the photocatalytic activity, parameter adjustments and a statistical data treatment were performed on TiO_2-anatase xerogel samples calcinated at 550˚C and 650˚C. The considered samples are listed in **Table 6** with their photocatalytic activity and their physico-chemical properties.

The main question is to determine if the photocatalytic activity of the TiO_2 xerogels doped with phosphor only depends on the particle size and on the specific area varying with amount of EDAP used during synthesis, or if the phosphor rate intrinsically influences the photocatalytic activity. In order to answer the question of the phosphor influence, three models have been adjusted on experimental data. The first model, named Model 1, describes the photocatalytic activity, A, as a function of the molar ratio P/Ti, P, only. The second model, named Model 2, describes A as a function of the particle size, d_a, and of the specific area, S_{BET}. The last model, named

Table 6. Physico-chemical properties and catalytic activity of all samples calcined at 550˚C and 650˚C.

	Sample	P (mol/mol)	d_a (nm)	S_{BET} ($m^2 \cdot g^{-1}$)	A (%)
1	Met-TiO_2-550	-	24	<5	21
2	Met-TiP/0.01-550	0.0028	14	40	18
3	Met-TiP/0.01-650	0.0056	19	35	29
4	Met-TiP/0.1-550	0.0710	8	105	44
5	Met-TiP/0.1-650	0.0724	8	90	57
6	Iso-TiP/0.1-550	0.0932	10	40	41
7	Iso-TiP/0.1-650	0.0246	13	45	25

Model 3, describes A as a function of the three previous variables P, d_a and S_{BET} simultaneously.

$$\text{Model 1:}\quad A = f_1(P) = a_0 + a_1 P + a_2 P^2 \tag{3}$$

$$\text{Model 2:}\quad A = f_2(d_a, S_{BET}) = b_0 + b_1 d_a + b_2 S_{BET} \tag{4}$$

$$\text{Model 3:}\quad A = f_3(P, d_a, S_{BET}) = c_0 + c_1 P + c_2 d_a + c_3 S_{BET} \tag{5}$$

where a_0, a_1, a_2 are the parameters of Model 1, b_0, b_1, b_2 are the parameters of Model 2 and c_0, c_1, c_2, c_3 are the parameters of Model 3.

In order to determine which model better fits on experimental data, a statistical Fisher F-test was performed with a 75% confidence interval. Models 1 and 2 include 3 parameters, while Model 3 includes 4 parameters. So the number of degrees of freedom of Models 1 and 2 and of Model 3 is respectively equal to 4 and 3 because 7 experimental points have been used for parameter adjustment. The estimators of the residual variance are equal to 68, 126 and 49 for Models 1, 2 and 3 respectively. The ratio between the estimators of the residual variance of Models 1 and 3 is equal to 1.39 and the ratio between the estimators of the residual variance of Models 2 and 3 is equal to 2.57. However, the Fischer variable $F(0.25, 4, 3)$ is equal to 2.4, which is greater than 1.39 and smaller than 2.57, meaning that Model 2 can be rejected while Models 1 and 3 cannot be discriminated. **Figure 6** compares the photocatalytic activity calculated with models 1, 2 and 3 with the experimental photocatalytic activity. Points corresponding to Models 1 and 3 are better aligned along the bisector than points corresponding to Model 2, in agreement with the statistical Fischer F-test. So because Model 2 describes A as a function of d_a and of S_{BET} only, it can be stated that phosphor intrinsically influences the photocatalytic activity, probably by extending the light adsorption to the visible range.

One last question remains till in mind: why Model 1 depending on P only, and Model 3 depending on P, d_a and S_{BET} simultaneously, are not statistically discriminatory. The explanation comes from the dependence of d_a and S_{BET} on P.

Figure 7 represents the experimental photocatalytic activity A as a function of P. A second degree expression corresponding to Model 1 and passing through a maximum is adjusted. According to Yu *et al.* [29], the maximum can be explained by the fact that a too high P value improves the formation of TiP_2O_7 species inhibiting the TiO_2 photocatalytic activity.

Because Model 1, depending on P only, and Model 3, depending on P, d_a and S_{BET}, are not statistically different, it seems that d_a and S_{BET} only depends on P. **Figure 8** represents the anatase particle size d_a as a function of P and the relation between d_a and P is modelled by:

$$d_a = d_0 + d_1 P + d_2 P^2 \tag{6}$$

where d_0, d_1, d_2 are the coefficients of the equation. The particle size d_a increases when P increases, reaches a maximum for a P value around 0.07 before decreasing for higher P values. The optimal P value of 0.07 corresponds to the maximum photocatalytic activity observed in **Figure 7**. Those results are in agreement with Zheng *et al.* observations that highlighted that above P equal to 0.08, the increase of P inhibits the particle growth [31].

Figure 9 represents the specific surface area, S_{BET}, as a function of P and the relation between S_{BET} and P is modelled by:

$$S_{BET} = e_0 + e_1 P + e_2 P^2 \tag{7}$$

where e_0 e_1, e_2 are the coefficients of the Equation (7). The specific surface area, S_{BET}, increases when P increases, reaches a maximum for a P value of around 0.06 before decreasing for higher P values. The optimal P value of 0.06 approximately corresponds to the maximum photocatalytic activity observed in **Figure 7**. Those results are in agreement with literature that places the optimal P value between 0.05 and 0.1 [29] [31].

So Equation (6) and Equation (7) describe d_a and S_{BET} as a function of P only, according to a second degree relation. Furthermore, Model 3 is linear with P, d_a and S_{BET}, meaning that Model 3 can be assimilated to a second degree equation as a function of P. This explains why Models 1 and 3 are not statistically discriminatory and proves that phosphor intrinsically influences the photocatalytic activity.

5. Conclusions

The TiO_2-anatase structure in P-doped TiO_2 xerogels appears after calcination at 550˚C and is always present af-

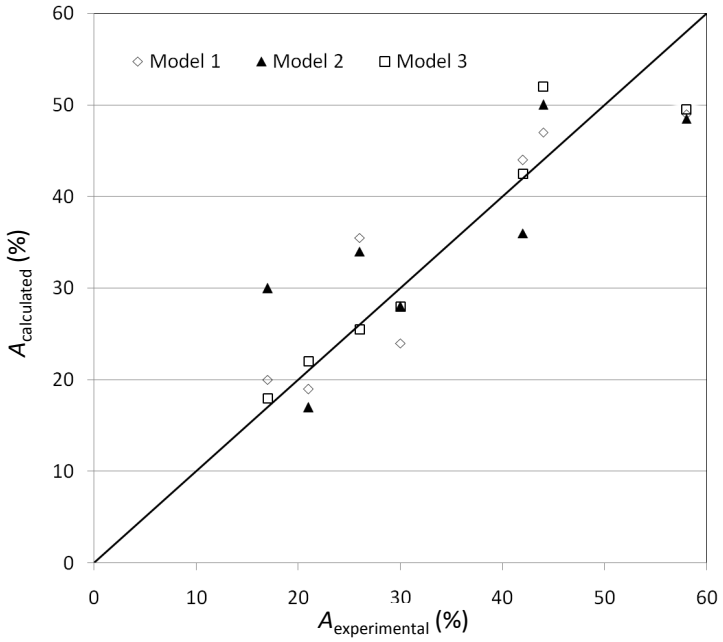

Figure 6. Parity diagram for Model 1 ($A = f_1(P)$) (◊), Model 2 ($A = f_2(d_a, S_{BET})$) (▲) and Model 3 ($A = f_3(P, d_a, S_{BET})$) (□).

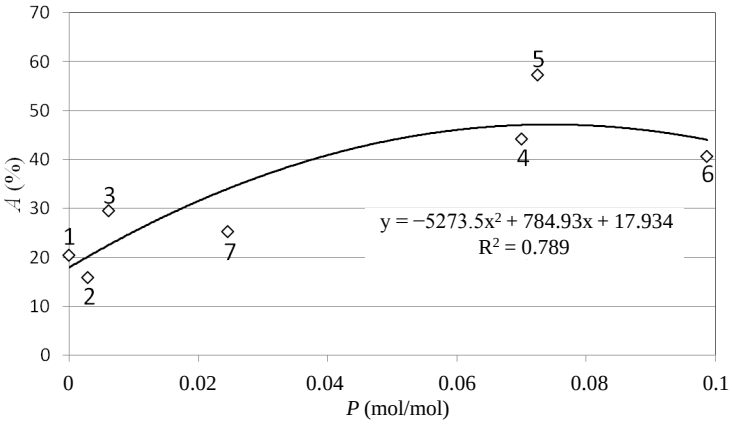

Figure 7. Photocatalytic activity as a function of P for the PN degradation. Points correspond to experimental data, the line corresponds to parameter adjustment and numbers correspond to samples listed in **Table 6**.

ter calcination at 650˚C, while the TiO_2-anatase in pure TiO_2 xerogels appears from 350˚C and after calcination at 650˚C, anatase is completely transformed in TiO_2-rutile. For photocatalytic *p*-nitrophenol degradation, P-doped TiO_2 xerogels are more active than pure TiO_2 xerogels. Indeed, the *p*-nitrophenol degradation percentage reachs 35% for the pure TiO_2 xerogel, while it reachs 55% for P-doped TiO_2 xerogels (sample Met-TiP/0.1-650).

In this study, it was established that the relations between the physico-chemical properties and the photocatalytic activity of P-doped TiO_2 xerogels strongly depend of the molar P/Ti ratio. The photocatalytic activity also depends to the size of TiO_2-anatase crystallites and to the specific surface area of xerogels: xerogels are even more active for the *p*-nitrophenol degradation that the size of TiO_2-anatase crystallites is small and the specific surface area is high.

Acknowledgements

Two of us (S.L.P and S.D.L.) are grateful to F.R.S.-F.N.R.S for their postdoctoral research and research asso-

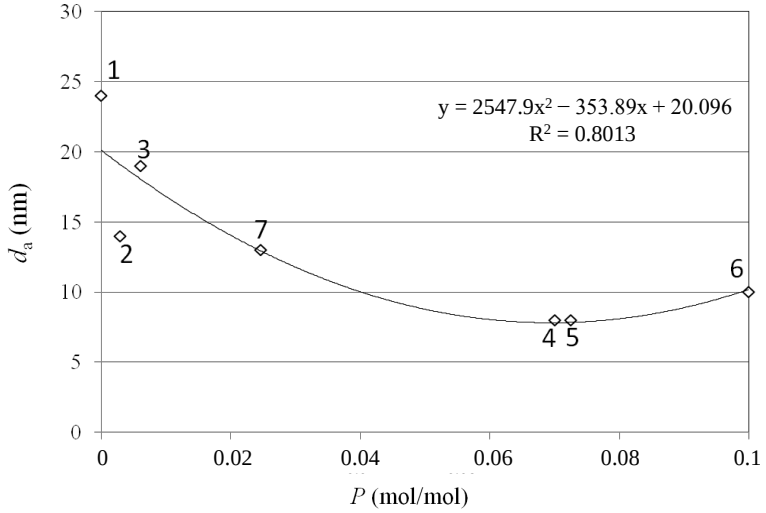

Figure 8. Diameter of TiO_2-anatase crystallites, d_a, as a function of *P*. Points correspond to experimental data, the line corresponds to parameter adjustment and numbers correspond to samples listed in **Table 6**.

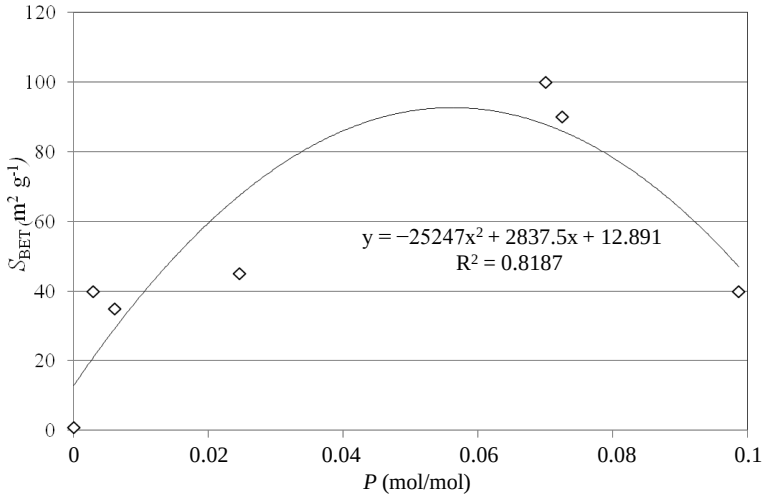

Figure 9. Specific surface area, S_{BET}, of TiO_2-anatase crystallites as a function of *P*. Points correspond to experimental data, the line corresponds to parameter adjustment and numbers correspond to samples listed in **Table 6**.

ciate positions respectively. One of us (L.T.) is grateful to the Belgian Fonds pour la Formation à la Recherche dans l'Industrie et dans l'Agriculture, F.R.I.A., and the University of Liege for a PhD grant. The authors would like to thank Pr. Jean-Paul Pirard, University of Liege (Belgium), and Pr. Dirk Poelman, University of Ghent (Belgium), for helpful discussions. The authors also acknowledge the Ministère de la Région Wallonne Direction Générale des Technologies, de la Recherche et de l'Energie, the Fonds de Recherche Fondamentale Collective and the Interuniversity Attraction Pole (IAP-P6/17), the FAME Network of Excellence and the French "Ministère des affaires étrangères et européennes" (PHC Tournesol) for financial supports.

References

[1] Fujishima, A., Rao, T.N. and Tryk, D.A. (2000) Titanium Dioxide Photocatalysis. *Journal of Photochemistry and Photobiology C*: *Photochemistry Reviews*, **1**, 1-21.

[2] Gaya, U.I. and Abdullah, A.H. (2008) Heterogeneous Photocatalytic Degradation of Organic Contaminants over Titanium Dioxide: A Review of Fundamentals, Progress and Problems. *Journal of Photochemistry and Photobiology C*:

Photochemistry Reviews, **9**, 1-12. http://dx.doi.org/10.1016/j.jphotochemrev.2007.12.003

[3] Mills, A. and Le Hunte, S. (1997) An Overview of Semiconductor Photocatalysis. *Journal of Photochemistry and Photobiology A*: *Chemistry*, **108**, 1-35. http://dx.doi.org/10.1016/S1010-6030(97)00118-4

[4] Lv, Y., Yu, L., Huang, H., Liu, H. and Feng, Y. (2009) Preparation, Characterization of P-Doped TiO_2 Nanoparticles and Their Excellent Photocatalystic Properties under the Solar Light Irradiation. *Journal of Alloys and Compounds*, **488**, 314-319. http://dx.doi.org/10.1016/j.jallcom.2009.08.116

[5] Lin, L., Zheng, R.Y., Xie, J.L., Zhu, Y.X. and Xie, Y.C. (2007) Synthesis and Characterization of Phosphor and Nitrogen Co-Doped Titania. *Applied Catalysis B*: *Environmental*, **76**, 196-202. http://dx.doi.org/10.1016/j.apcatb.2007.05.023

[6] Xu, L., Tang, C.Q., Qian, J., Huang, Z. B. (2010) Theoretical and Experimental Study on the Electronic Structure and Optical Absorption Properties of P-Doped TiO_2. *Applied Surface Science*, **256**, 2668-2671. http://dx.doi.org/10.1016/j.apsusc.2009.11.046

[7] Yu, J., Yu, J.C., Ho, W., Leung, M.P.K., Cheng, B., Zhang, G. and Zhao, X. (2003) Effects of Alcohol Content and Calcination Temperature on the Textural Properties of Bimodally Mesoporous Titania. *Applied Catalysis A*: *General*, **255**, 309-320. http://dx.doi.org/10.1016/S0926-860X(03)00570-2

[8] Stafford, U., Gray, K.A., Kamat, P.V. and Varma, A. (1993) An *in Situ* Diffuse Reflectance FTIR Investigation of Photocatalytic Degradation of 4-Chlorophenol on a TiO_2 Powder Surface. *Chemical Physics Letters*, **205**, 55-61. http://dx.doi.org/10.1016/0009-2614(93)85166-L

[9] Yoo, K.S., Lee, T.G. and Kim, J. (2005) Preparation and Characterization of Mesoporous TiO_2 Particles by Modified Sol-Gel Method Using Ionic Liquids. *Microporous and Mesoporous Materials*, **84**, 211-217. http://dx.doi.org/10.1016/j.micromeso.2005.05.029

[10] Simonsen, M. and Søgaard, E. (2010) Sol-Gel Reactions of Titanium Alkoxides and Water: Influence of pH and Alkoxy Group on Cluster Formation and Properties of the Resulting Products. *Journal of Sol-Gel Science and Technology*, **53**, 485-497. http://dx.doi.org/10.1007/s10971-009-2121-0

[11] Terabe, K., Kato, K., Miyazaki, H., Yamaguchi, S., Imai, A. and Iguchi, Y. (1994) Microstructure and Crystallization Behaviour of TiO_2 Precursor Prepared by the Sol-Gel Method Using Metal Alkoxide. *Journal of Materials Science*, **29**, 1617-1622. http://dx.doi.org/10.1007/BF00368935

[12] Li, Z., Hou, B., Xu, Y., Wu, D., Sun, Y., Hu, W. and Deng, F. (2005) Comparative Study of Sol-Gel-Hydrothermal and Sol-Gel Synthesis of Titania-Silica Composite Nanoparticles. *Journal of Solid State Chemistry*, **178**, 1395-1405. http://dx.doi.org/10.1016/j.jssc.2004.12.034

[13] Wang, C.Y., Bahnemann, D.W. and Dohrmann, J.K. (2000) A Novel Preparation of Iron-Doped TiO_2 Nanoparticles with Enhanced Photocatalytic Activity. *Chemical Communications*, **16**, 1539-1540. http://dx.doi.org/10.1039/b002988m

[14] Sibu, C.P., Kumar, S.R., Mukundan, P. and Warrier, K.G.K. (2002) Structural Modifications and Associated Properties of Lanthanum Oxide Doped Sol-Gel Nanosized Titanium Oxide. *Chemistry of Materials*, **14**, 2876-2881. http://dx.doi.org/10.1021/cm010966p

[15] Braconnier, B., Páez, C.A., Lambert, S., Alié, C., Henrist, C., Poelman, D., Pirard, J.P., Cloots, R. and Heinrichs, B. (2009) Ag- and SiO_2-Doped Porous TiO_2 with Enhanced Thermal Stability. *Microporous and Mesoporous Materials*, **122**, 247-254. http://dx.doi.org/10.1016/j.micromeso.2009.03.007

[16] Bodson, C.J., Lambert, S.D., Alié, C., Cattoën, X., Pirard, J.P., Bied, C., Manb, M.W.C. and Heinrichs, B. (2010) Effects of Additives and Solvents on the Gel Formation Rate and on the Texture of P- and Si-Doped TiO_2 Materials. *Microporous and Mesoporous Materials*, **134**, 157-164. http://dx.doi.org/10.1016/j.micromeso.2010.05.021

[17] Brinker, C.J. and Scherer, G.W. (1990) Sol-Gel Science: The Physics and Chemistry of Sol-Gel Processing. Academic Press, San Diego.

[18] Bergeret, G. and Gallezot, P. (1997) Particle Size and Dispersion Measurements. In: Ertl, G., Knözinger, H., Schuth, F. and Weitkamp, J., Eds., *Handbook of Heterogeneous Catalysis*, Wiley-VCH, Weinheim, 439-464.

[19] Kubelka, P. and Munk, F. (1931) Ein Beitrag Zur Optik Der Farbanstriche. *Zeitschrift für Technische Physik*, **12**, 593-601.

[20] Tauc, J., Grigorovici, R. and Vancu, A. (1966) Optical Properties and Electronic Structure of Amorphous Germanium. *Physica Status Solidi* (*b*), **15**, 627-637. http://dx.doi.org/10.1002/pssb.19660150224

[21] Himmelblau, D.M. (1970) Process Analysis by Statistical Methods. Wiley, New York.

[22] Press, W.H., Flannery, B.P., Teukolsky, S.A. and Vetterling, W.T. (1990) Numerical Recipes in C—The Art of Scientific Computing. Cambridge University Press, Cambridge.

[23] Pirard, S., Pirard, J.P., Heyen, G., Schoebrechts, J.P. and Heinrichs, B. (2011) Experimental Procedure and Statistical

Data Treatment for the Kinetic Study of Selective Hydrodechlorination of 1,2-Dichloroethane into Ethylene over a Pd-Ag Sol-Gel Catalyst. *Chemical Engineering Journal*, **173**, 801-812. http://dx.doi.org/10.1016/j.cej.2011.07.002

[24] Stojanović, B., Marinković, Z., Branković, G. and Fidančevska, E. (2000) Evaluation of Kinetic Data for Crystallization of TiO_2 Prepared by Hydrolysis Method. *Journal of Thermal Analysis and Calorimetry*, **60**, 595-604. http://dx.doi.org/10.1023/A:1010107423825

[25] Lachheb, H., Houas, A. and Herrmann, J.M. (2008) Photocatalytic Degradation of Polynitrophenols on Various Commercial Suspended or Deposited Titania Catalysts Using Artificial and Solar Light. *International Journal of Photoenergy*, **2008**, Article ID: 497895, 9 Pages.

[26] Lecloux, A.J. (1981) Texture of Catalysts. In: Anderson, J.R. and Boudart, M., Eds., *Catalysis*: *Science and Technology*, Vol. 2, Springer, Berlin, 171-230.

[27] Li, F.F., Jiang, Y.S., Xia, M.S., Sun, M.M., Xue, B., Liu, D.R. and Zhang, X.G. (2009) Effect of the P/Ti Ratio on the Visible-Light Photocatalytic Activity of P-Doped TiO_2. *The Journal of Physical Chemistry C*, **113**, 18134-18141. http://dx.doi.org/10.1021/jp902558z

[28] Körösi, L., Papp, S., Bertóti, I. and Dékány, I. (2007) Surface and Bulk Composition, Structure, and Photocatalytic Activity of Phosphate-Modified TiO_2. *Chemistry of Materials*, **19**, 4811-4819. http://dx.doi.org/10.1021/cm070692r

[29] Yu, H.F. (2007) Photocatalytic Abilities of Gel-Derived P-Doped TiO_2. *Journal of Physics and Chemistry of Solids*, **68**, 600-607. http://dx.doi.org/10.1016/j.jpcs.2007.01.050

[30] Myller, A.T., Karhe, J.J. and Pakkanen, T.T. (2010) Preparation of Aminofunctionalized TiO_2 Surfaces by Binding of Organophosphates. *Applied Surface Science*, **257**, 1616-1622. http://dx.doi.org/10.1016/j.apsusc.2010.08.109

[31] Zheng, R.Y., Lin, L., Xie, J.L., Zhu, Y.X. and Xie, Y.C. (2008) State of Doped Phosphorus and Its Influence on the Physicochemical and Photocatalytic Properties of P-Doped Titania. *The Journal of Physical Chemistry C*, **112**, 15502-15509. http://dx.doi.org/10.1021/jp806121m

Scientific Research Publishing (SCIRP) is one of the largest Open Access journal publishers. It is currently publishing more than 200 open access, online, peer-reviewed journals covering a wide range of academic disciplines. SCIRP serves the worldwide academic communities and contributes to the progress and application of science with its publication.

Other selected journals from SCIRP are listed as below. Submit your manuscript to us via either submit@scirp.org or Online Submission Portal.